JOURNAL OF GEOPHYSICAL RESEARCH, VOL. , NO. , PAGES 1–22,

Kelvin wave signatures in stratospheric trace constituents, Part I: ozone, nitrous oxide, methane, and CFC-12

Philip W. Mote and Timothy J. Dunkerton

Northwest Research Associates, Bellevue, Washington

T.J. Dunkerton and P.W. Mote, Northwest Research Associates, PO Box 3027, Bellevue WA 98009. (mote@nwra.com, tim@nwra.com)

Abstract. Connections, sometimes tenuous, have previously been noted between stratospheric Kelvin waves and several stratospheric trace constituents. The present study finds evidence of Kelvin wave signatures in ozone from the Microwave Limb Sounder (MLS) and Cryogenic Limb Array Etalon Spectrometer (CLAES) instruments aboard the Upper Atmosphere Research Satellite. Predominant variations near 10 days are associated with a Kelvin wave mode previously identified in MLS temperature. Variations in CLAES methane, nitrous oxide, and CFC-12 each show some evidence of influence by this Kelvin mode. A companion paper examines the more complicated issue of water vapor, whose vertical structure varies seasonally. The results presented here show that the observing characteristics of the instrument can influence the derived structure and properties of Kelvin waves.

1. Introduction

On time scales less than 90 days, the dominant features in the tropical stratosphere are produced by atmospheric Kelvin waves [e.g., *Wallace and Kousky*, 1968]. Kelvin waves, which are equatorially trapped, perturb the temperature, wind, and trace constituent fields; they also influence stratosphere-troposphere exchange [*Fujiwara et al.,* 1998, 2001]. Observations from space-based instruments have shown the structure of Kelvin waves in temperature and have helped illuminate their influence on trace constituents. *Randel* [1990] examined data from the Limb Infrared Monitor of the Stratosphere (LIMS) for water vapor (H_2O), ozone (O_3), nitric acid (HNO_3), and nitrogen dioxide (NO_2). Randel found reasonable relationships between temperature perturbations and perturbations in O_3 and HNO_3, but very small and retrieval-dependent perturbations in H_2O and NO_2, with H_2O's weak signal confined to the lower stratosphere. *Kawamoto et al.* [1997] also examined LIMS data for O_3 and H_2O, and, like Randel, found a weak signal of H_2O perturbations in the lower stratosphere. *Shiotani et al.* [1997] looked for Kelvin wave signatures in H_2O and O_3 observations from the Cryogenic Limb Array Etalon Spectrometer (CLAES), aboard the Upper Atmosphere Research Satellite (UARS), but reported that they "could not find significant signals" in these fields. *Canziani et al.* [1994, 1995, 1998] described variations in MLS temperature and ozone, showing that the relationship between the two fields was generally as expected from theoretical and modelling studies. Using data taken by the CRISTA instrument flying during two NASA Space Shuttle missions, each lasting just over a week, *Smith et al.* [2002] found Kelvin wave-like features in O_3, CFC-11, HNO_3, N_2O, and CH_4 that were correlated with temperature perturbations.

Mote et al. [2002] (hereinafter M02), described Kelvin wave variations in MLS temperature data. This study extends their work by describing the variations in several trace constituents from the MLS and CLAES instruments. We examine temperature and ozone data from both MLS and CLAES, and methane, nitrous oxide, and chlorofluorocarbon (CFC)-12 from CLAES. In a companion paper we examine MLS water vapor data. While many other trace constituents are available on UARS, these trace constituents were chosen because their vertical profiles (a crucial determinant of Kelvin wave signatures) are quite different. Methane has almost no gradient in the lower stratosphere, but decreases sharply in the upper stratosphere; nitrous oxide and CFC-12 decrease steadily from the lower stratosphere to values near zero in the upper stratosphere; the gradient of ozone changes sign in the middle stratosphere; and water vapor has a seasonally varying vertical profile in the lower stratosphere, with two or even three changes in sign of its vertical gradient.

2. Data

The Upper Atmosphere Research Satellite (UARS) [*Reber et al.,* 1993] was launched in September 1991 and collected data for ten years until science observations ceased for budgetary, not scientific or engineering, reasons. UARS is in an orbit inclined 57° to the equator at an altitude of 585 km. Owing to orbit precession, approximately every 36 days the spacecraft must perform a yaw maneuver.

Constituent data are provided on a grid with 6 levels per factor of 10 in pressure, i.e., 100, 68.1, 46.4, 31.6, 21.5, 14.7, 10 hPa, and so on. The vertical spacing of these grid levels is approximately 2.7 km. CLAES and MLS have similar viewing geometry and frequency

of profiles, and for both data sets we use L3AT data (in which data are interpolated to a standard set of profiles along the viewing track) from the most recent version.

For this study we focus on the tropics, i.e., latitudes between 27.5° S and 27.5° N. The profile data are first averaged using bins of width 24° longitude and 5° latitude for each day. While the longitudinal resolution may seem very coarse, it is ample for resolving the features of interest, which tend to have most of their power in zonal wavenumbers 1 and 2. On most days there are over 500 profiles within this latitude band (out of a global total of over 1300 per day), and consequently the typical bin contains about three profiles. Since we are focusing on time scales longer than ∼4 days and on a phenomenon with essentially no diurnal dependence, the results should be insensitive to the fact that we have ignored the local time of observation.

The time period studied here stretches from July 1992 to late April 1993, the period of record with the densest, highest-quality trace constituent measurements. All data are bandpass filtered (4–90 days), to remove the seasonal cycle and variations at high frequencies that might be affected by aliasing with the satellite's orbit.

2.1. Microwave Limb Sounder

The Microwave Limb Sounder (MLS) [*Barath et al.*, 1993] retrieves temperature and constituent data from microwave emissions using three radiometers (at 63, 183, and 205 GHz). Version 5 (V5) data are used for temperature and ozone [*Livesey et al.*, 200X]. Small temporal gaps (all but two of which are only one day long) are filled by linear interpolation in time for analyses, but not in Figure 2 where the gaps are visible.

2.1.1. MLS temperature.

The MLS V5 algorithm retrieves temperatures above the 68 hPa pressure level on every UARS surface, but the range of most reliable temperatures is 32 – 0.46 hPa; MLS still contributes some information at 46 hPa, but very little at 68 hPa. The Kelvin wave signature in this data set was described by *Mote et al.* [2002]; they found coherent Kelvin wave variations down to 68 hPa, despite the poor data quality there. The mean tropical profile of MLS temperature is shown in Figure 1a.

Figure 1

2.1.2. MLS ozone.

Two separate MLS ozone products [*Froidevaux et al.,* 1996] are retrieved, one using the 205 GHz radiometer and one using the 183 GHz radiometer. The 183-GHz radiometer failed in late April 1993. Here we use only data from the 205 GHz radiometer, as these data are more accurate in the stratosphere [*Froidevaux et al.,* 1996]. Accuracy is very good (order of 5%) in most of the stratosphere, but errors increase sharply approaching the tropical tropopause (exceeding 50% at 100 hPa) owing to the very low ozone values there. We use data from 46 to 0.68 hPa (Figure 1c).

2.2. CLAES

The Cryogenic Limb Array Etalon Spectrometer (CLAES) retrieves temperature and constituent data from infrared emissions [*Roche et al.*, 1993]. An array of stacked detectors, each pointing at a different 2.5-km-thick vertical slice of the limb, provided simultaneous vertical coverage from 10 to 60 km. To prevent the instrument's own thermal emissions from interfering with the atmospheric signal, the instrument was cooled with cryogens; the cryogens finally evaporated on May 5, 1993, ending the CLAES period of observations. Nine blocking filters each pass a certain narrow frequency band of incoming infrared radiation. Temperature is retrieved using filter 8 (centered on 792 cm^{-1}) [*Gille*

et al., 1996], ozone using filter 8 and filter 9 (780 cm^{-1}) [*Bailey et al.,* 1996], CFC-12 (CF_2Cl_2) using filter 5 (923 cm^{-1}) [*Nightingale et al.,* 1996], and methane (CH_4) and nitrous oxide (N_2O) using filter 4 (1257 cm^{-1}) [*Roche et al.,* 1996]. The validation papers cited here referred to CLAES V7; in this paper we use CLAES V9, and note below any significant changes from the V7 data.

Around the time of each UARS yaw maneuver, the CLAES instrument's aperture door was closed for several days to protect the instrument from sunlight [*Bailey et al.,* 1996]. These data gaps are sufficiently frequent, lengthy, and periodic that we do not attempt to fill the gaps by interpolation as we do with MLS.

2.2.1. CLAES temperature.

Correlative measurements for temperature are far more numerous than for trace constituents, and include radiosondes, ground-based lidar, and the reanalyses of the National Centers for Environmental Prediction (NCEP) and the United Kingdom Meteorological Office (UKMO). *Gille et al.* [1996] note a global cold bias of about 2K in V7; the bias in V9 is near zero (CLAES web site). They also note differences with NCEP and UKMO in latitude-pressure sections, which they attribute to tropical waves of the sort examined in this paper; such waves would elude the nadir-viewing TOVS instrument that forms the basis for the reanalysis data. Indeed, as M02 noted, NCEP and UKMO data do not exhibit the Kelvin wave variations seen in MLS.

The CLAES temperature retrieval extends down to the 316 hPa level, and errors with respect to radiosondes are small (1-2 K) at 146 and 215 hPa. CLAES provides estimates of temperature well below the lowest valid MLS level, though we presume the measurements will be obscured by clouds and hence biased toward cloud-free conditions. At the levels

where both CLAES and MLS report temperature values, CLAES is consistently higher (Figure 1a) and has more variance (Figure 1b)

2.2.2. CLAES ozone.

CLAES ozone measurements agree well with correlative measurements throughout the altitude range of the stratosphere [*Bailey et al.,* 1996], though most of these correlative measurements were taken in middle or high latitudes. In the tropics below the peak in the ozone profile, possible contamination by volcanic aerosol is a concern, but the good agreement with MLS ozone (Figure 1c) is reassuring, because MLS measurements are unaffected by aerosol. The differences between MLS and CLAES in the mean profiles are consistent with the slight high bias of CLAES ozone near 10 hPa and low bias in the upper stratosphere [*Bailey et al.,* 1996]. Tropical ozone values below 20 hPa are several tenths of a ppmv lower in V9 than in V7, with large percentage reductions (greater than 50%) just above the tropopause (CLAES web site); these reductions bring it into line with MLS observations.

2.2.3. CLAES methane.

Correlative measurements indicate that CLAES methane is generally reliable in the middle and upper stratosphere, but there were very few correlative measurements below 20 hPa and none in the tropics except the ATMOS instrument aboard the space shuttle [*Roche et al.,* 1996]. The profile of methane (Figure 1e) shows a local maximum at about 20 hPa. With near-monotonic increases with time in the troposphere, no sources in the stratosphere and a photochemical sink in the upper stratosphere, the time-mean profile of methane should decrease monotonically upward from the tropical tropopause; the local maximum observed is a departure from expected values. Although a disturbance

in stratospheric circulation by the Mt. Pinatubo eruption is a possible explanation, the modeling work of *Considine et al.* [200X] suggests that the changes in circulation would be insufficient to generate a local maximum as observed in CLAES data. The facts that (1) other CLAES constituents show a similar feature (Figures 1g, 1i; though the local maximum is not always at the same altitude), (2) methane data from the Halogen Occultation Experiment show no such feature in 1992 and 1993, and (3) the feature was stronger in V7 data (CLAES web site), all suggest that it may be a retrieval problem associated with the vestiges of the Pinatubo aerosol cloud. Combined with the sharp increase in variance in lower levels (Figure 1f), this feature casts suspicion on the methane measurements at altitudes below 22 hPa. Data quality is expected to be higher for V9 than for V7; at almost every level, V9 data have lower globally averaged errors than V7, with respect to correlative data.

2.2.4. CLAES nitrous oxide (N_2O).

Methane and nitrous oxide are both retrieved by the same filter (4) on CLAES. The vertical profile of CLAES nitrous oxide (Figure 1g) is similar to methane, including the unexplained local maximum in the lower stratosphere and decline to low values in the upper stratosphere. They have similarly limited correlative measurements in the tropics, but globally, the CLAES V7 N_2O data are biased slightly low (by less than 15%) below 7 hPa. The V9 data are substantially lower than V7 in the tropical lower stratosphere and have a more accentuated local maximum, though globally the differences between V9 and correlative data are smaller (CLAES web site).

2.2.5. CLAES CFC-12 (CF_2Cl_2).

The retrieval of CF_2Cl_2 is described by *Nightingale et al.* [1996]. There are far fewer correlative data for CF_2Cl_2 than for the other constituents. CLAES CF_2Cl_2 is 5–20% lower than three balloon soundings at 35° N, but agrees within a few percent with several coincident ATMOS soundings in the southern hemisphere. *Nightingale et al.* [1996] give highest marks to data between 68 and 10 hPa, and report that values in the tropics between 100 and 22 hPa "may be biased low by up to 14%." In V9, tropical values are substantially larger (25–35%) than V7 (CLAES web site).

CF_2Cl_2 is very similar to N_2O in its rapid drop to near-zero values between the lower stratosphere and the upper stratosphere (Figure 1i) and also its local maximum of variance near 10 hPa (Figure 1j).

3. Description of variations in temperature and trace constituents

As in M02, the three-dimensional stratospheric variations in the fields of interest (temperature, ozone, methane, nitrous oxide, and CFC-12) are initially reduced to one dimension by taking the projection of the field onto the cosine of longitude, along the equator (Figure 2). The same projection is done for the sine of longitude; these are not shown, but are substantially similar to those for the cosine.

Figure 2

Downward-propagating features are clearly evident in MLS temperature (Figure 2a) and were discussed by M02. Of particular interest are the large-amplitude events in September 1992 and January-February 1993. M02 identified two distinct modes in the $k = 1$ MLS temperature variations shown in Figure 2a, and verified that both satisfied the dispersion relation for Kelvin waves. The one that is most obvious in Figure 2a has period near 10 days, vertical wavelength 20 km in the upper stratosphere, and horizontal phase speed 48 ms^{-1}. The less obvious mode has a period of 6.5 days, vertical wavelength 23 km, and

horizontal phase speed 71 ms^{-1}. It has largest amplitude in December 1992 and January 1993.

There is a very good correspondence between the variations in CLAES temperature (Figure 2b) and the variations in MLS temperature just discussed. CLAES has the advantage of extending into the troposphere, and it appears that the variations noted in the MLS data are linked to variations at 100 hPa. In a companion paper [*Mote et al.,* 200X], we show that these coherent variations continue into the upper troposphere.

MLS ozone data (Figure 2c) also clearly show downward-propagating features, and most correspond well to the temperature variations. However, in the lower stratosphere, the predominant variations have longer period and smaller vertical phase speed. These features are especially prominent in August-September 1992 and also appear in late January 1993. It is difficult to identify by eye the expected phase reversal that should accompany the change in sign of the vertical gradient at around 10 hPa (Figure 1c).

Unfortunately, CLAES ozone data Figure 2d are too noisy to reveal clearly the same sorts of variations that are shown in Figure 2c. There are intriguing suggestions of the same descending features, especially in August-September 1992, as those in MLS. The variance is larger than with MLS ozone data (Figure 1d).

The story is similar with other CLAES constituents (Figures 2e–g): downward-propagating features are evident to differing degrees. The downward-propagating features are clearest in methane in the upper stratosphere during the large-amplitude events. Mere hints of these features are visible in nitrous oxide (Figure 2f) but not at all in CFC-12 (Figure 2g). Statistical analysis of these data reveal more connections than are evident in Figure 2.

3.1. Spectral analysis

Gaps in CLAES data (Figure 2) are too numerous for spectral analysis to work well, but MLS data are nearly continuous. We perform spectral analysis by wavenumber and frequency at each of the latitudes and altitudes in the study domain, as in M02, but now for both temperature and ozone from MLS. For temperature (Figure 3), there is a sharp spectral peak at about 10 days, part of a band of spectral power between roughly 7.5 and 11.5 days. Note that the extended empirical orthogonal function (EEOF) analysis of the same data by M02 led to a spectral peak at about 9.6 days. There are other peaks in the intraseasonal range and near 6 days, corresponding to the second mode identified by M02.

Figure 3

Spectral power is strongly concentrated in wavenumber 1 (Figure 3b), especially for eastward (positive) wavenumber 1. The meridional distribution (Figure 3c) shows a peak at the equator, diminishing toward the subtropics. Beyond 15° (not shown), power rises again owing to midlatitude waves.

The vertical profile of spectral power (Figure 3d) shows a near-monotonic increase with height, despite the decrease in overall variance from 100 hPa to 22 hPa (Figure 1b). The overall variance includes seasonal and zonal variations, which are excluded from the analysis here; seasonal variations in temperature are strongest near the tropopause and diminish sharply with altitude [*Reed and Vlcek*, 1969], accounting for the differences between Figure 1b and Figure 3d. At every level the spectral power in the 5–30 day band accounts for nearly all of the power in the frequency band analyzed here (roughly 4–90 days).

For ozone, the largest spectral peak (Figure 4a) is near 10 days, as for temperature,

Figure 4

but the rest of the spectrum is somewhat redder (more variance at low frequencies) for ozone than for temperature. The wavenumber dependence (Figure 4b) is similar to that for temperature, with eastward $k = 1$ dominant followed by westward $k = 1$ and substantially less power at higher wavenumbers. The latitude dependence of $k = 1$ spectral power (Figure 4c) is also similar to that for temperature, peaked at the equator and falling to about half that value at 15° latitude.

Only the vertical dependence (Figure 4d) of spectral power is substantially different from that of temperature; maxima in the lower and upper stratosphere are separated by a minimum at the altitude of the ozone maximum, as expected (since perturbations depend on $\partial O_3/\partial z$, and $\partial O_3/\partial z \simeq 0$ near 10 hPa). *Randel* [1990] obtained a similar result using LIMS V5 data, but the results were quite different in LIMS V4 data (his Figure 3). There are two reasons the spectral peak for ozone in the lower stratosphere should be larger than the one in the upper stratosphere even though the spectral peak for temperature in the upper stratosphere is larger: first, the vertical gradient is relatively larger in the lower stratosphere (this can be seen by plotting dO_3/dT versus altitude) and second, the photochemical timescale for ozone is short in the upper stratosphere, so it adjusts rapidly to perturbations in temperature [*Randel*, 1990].

Having examined the variations in temperature and ozone separately, we now examine their co-variation. Using the technique outlined by *von Storch and Zwiers* [2001], we calculate coherence squared for MLS temperature and ozone. These are calculated for both sine and cosine components, then averaged. Figure 5a shows how the temperature-ozone coherence squared depends on altitude and period. Since both fields have a spectral peak near 10 days, it is no surprise that the largest peak in the coherence squared is also

Figure 5

near 10 days. It gives the appearance of tending toward shorter periods as altitude increases, and there is a minimum at 10–20 hPa as expected. There is also a broad, shallow peak in the lower stratosphere at about 17 days (see Figure 4; the feature appears as the second pair of EEOFs of ozone, not shown) and a sharp peak at about 6 days (see Figure 3) in the upper stratosphere.

For the 10-day wave at most levels, the quadrature spectra exceed the cospectra in absolute value, leading to a phase relationship that tends to be closer to $\pm 90°$ than to $0°$ or $180°$ (since the phase is the arctangent of the quadrature spectrum over the cospectrum). *Randel* [1990] found, in agreement with linear theory, that the phase difference between temperature and ozone was generally close to zero below 30 km and close to $180°$ above 40 km, and although the MLS data also suggest a $180°$ phase shift, in our results it is between $+90°$ and $-90°$. The phase relationship will become clearer in the next subsection. For the 6-day wave, the phase is less well defined.

3.2. Regression

M02 calculated extended empirical orthogonal functions (EEOFs) of MLS temperature data and used the first principal component (PC) to find the three-dimensional structure of the 10-day Kelvin mode by regression. We use the same reference time series, i.e., the first PC of MLS temperature data, and regress MLS and CLAES temperature, MLS and CLAES ozone, and CLAES CH_4, N_2O, and CF_2Cl_2 (Figure 6). Regression analysis is more suitable for the gappy CLAES data than analysis requiring continuous time series, e.g., spectral analysis or EEOF analysis.

Figure 6

The amplitude of the CLAES variations is slightly greater than for the MLS variations, especially for negative temperature anomalies which are about twice as big as those in

MLS. A partial explanation for the higher amplitude is the larger overall variance of CLAES temperatures (Figure 1b); though the ratio of variances is smaller than the ratio of 10-day Kelvin wave amplitudes, it is possible that for the 10-day band the ratio of variances is larger than for other bands (compare Figure 2a, 2b). A more perplexing difference between MLS and CLAES occurs in the lowermost stratosphere, where the phase lines no longer coincide between the two datasets. A possible explanation is that the EEOF calculation in MLS emphasized the upper stratosphere, and when performing regression, other variance can creep in; the lower stratospheric variations in CLAES may not be as coherent with the upper stratospheric variations as is the case in MLS. A more likely explanation lies in the differing vertical resolutions of the two instruments: CLAES precision is best at 100 hPa [*Gille et al.,* 1996] but MLS loses temperature sensitivity in the lower stratosphere and the retrieved profile is smoothed, hence decreasing the resolvable vertical scale [D. Wu, pers. communication, 2002]. The fact that the CLAES anomalies extend to the tropopause (100 hPa) is an intriguing possible connection to stratosphere-troposphere exchange that are explored in a companion paper [*Mote et al.,* 200X].

MLS ozone (Figure 6c) offers only hints of a relationship to temperature, though these will become clearer shortly. The phase lines seem to have roughly the same slope as for temperature, and there are hints of a sign change at the ozone maximum (10 hPa). The surprising results in Figure 5c are brought into focus here, with some of the maxima and minima occurring not on the 0° and 180° phase lines but between them. It is still not clear why these results depart from the expected in-phase relationship in the lower stratosphere and out-of-phase relationship in the upper stratosphere.

All of these features are clearer in CLAES ozone (Figure 6d), revealed by the regression analysis despite the difficulty of identifying them visually in Figure 2. The most prominent feature starts at 0° longitude, 21.5 hPa, as a negative anomaly approximately in phase with temperature; just above 10 hPa, it changes sign and is roughly out of phase with temperature. Along other phase lines, one can see similar features, though not as consistently. The CLAES ozone data provide a guide for identifying consistent features in MLS ozone. As with temperature, the variations in ozone are larger in CLAES data than MLS data, owing perhaps in part to larger overall variance (Figure 1d).

For CLAES methane (Figure 6e), little relationship with temperature is seen. Variations are weak in the lower stratosphere, where the vertical gradient is near zero and (at lowest levels) data are suspect (Figure 1e). The largest features in the upper stratosphere only follow the phase lines in the eastern hemisphere, though there is no physical reason for such selectivity.

Results for CLAES nitrous oxide (Figure 6f) are clearer, owing to its near-constant vertical gradient (Figure 1g). Perturbations line up quite well with the phase lines and are of the expected sign, i.e., opposite to that of temperature. The pattern breaks down in the lowest part of the stratosphere where, as with methane, the vertical gradient changes sign. In the upper stratosphere, the variations become very small as the background values of nitrous oxide approach zero (Figure 1g).

Finally, CFC-12 (Figure 6g) shows some features consistent with Kelvin wave signature above about 20 hPa, especially the positive anomaly centered at about 7 hPa and 180°. At this altitude the absolute variance of CFC-12 (Figure 1j) is a maximum, although the relative variance increases monotonically above 46 hPa). As with nitrous oxide, the signal

weakens in the upper stratosphere as the background values of CFC-12 approach zero (Figure 1i).

4. Conclusions

UARS data offer another look at the influence of Kelvin waves on stratospheric trace constituents. The roughly 10-day Kelvin wave mode identified by M02 appears also in the ozone, methane, nitrous oxide, and CFC-12 data, as revealed variously in Figure 2 (especially September 1992 and January-February 1993) and by the coherence and regression calculations in Figures 3 and 6 (and also EEOFs, not shown). The different techniques reveal Kelvin wave signatures better for different constituents: for example, the time-height plots in Figure 2 show the signatures more clearly for methane than does regression, while regression shows the signatures more clearly for nitrous oxide.

Kelvin waves are the dominant mode of tropical intraseasonal (4–90 days) variability in the stratosphere, for both temperature and ozone (Figures 3 and 4), with sharp spectral peaks at around 10 days for $k = 1$, and with a maximum variance at the equator. Other trace constituents, like CH_4, N_2O, and CF_2Cl_2, probably have similar spectral characteristics, but these constituents are measured only by CLAES and spectral analysis does not work well for CLAES data owing to the long and frequent gaps.

The response to Kelvin waves of these other long-lived trace constituents depends on their vertical profile. For nitrous oxide and CFC-12, which have large and near-constant vertical gradients above about 30 hPa, the signature of Kelvin waves is fairly clear and is consistent with the temperature variations (i.e., of opposite sign owing to the opposite sign of the vertical gradients). For methane, whose vertical gradient is small below about 7 hPa, results were ambiguous: the variations are clear (Figure 2e) but difficult to link

statistically with temperature (Figure 6e). A companion paper examines the case of water vapor, whose complex and seasonally varying vertical profile makes the identification of Kelvin wave influence even more difficult.

Important differences appear when the same field is examined from two different satellite datasets. CLAES data (both temperature and ozone) showed generally larger responses to the same Kelvin wave than did MLS data. Though the phases appeared to be similar for the two datasets for ozone, for temperature there were significant differences in the lower stratosphere, possibly owing to different vertical resolution there, with CLAES more likely to be correct. A companion paper explores the possibility that these Kelvin waves influence stratosphere-troposphere exchange and the moisture content of air entering the stratosphere.

Ground-based observations of stratospheric Kelvin waves can resolve much finer vertical scales, and such observations paint a somewhat different picture of Kelvin wave behavior with higher vertical and zonal wavenumbers (e.g., *Holton et al.*, 2001). This implies that the dominant Kelvin mode in any dataset depends on the observing characteristics of the instrument, a point made by *Alexander* [1998] for gravity waves. Although MLS and CLAES have similar viewing geometries (cool-side, limb-viewing) and vertical resolution, they end up with subtle but important differences in the structure of retrieved Kelvin waves (Figure 6). Future satellite missions with high vertical resolution, notably EOS-MLS and HIRDLS, may yield different leading modes; in any case, they will afford a more comprehensive look at variations in temperature and important trace constituents.

Acknowledgments. Aiden Roche provided helpful comments on an earlier draft of this manuscript, especially with regards to CLAES data. We thank Dong Wu for helpful

discussions, and gratefully acknowledge the accomplishments of the MLS and CLAES instrument teams. This work was supported by NASA contracts NAS1-99130, NAS5-98078, and NAS5-01154.

References

Alexander, M.J., Interpretations of observed climatological patterns in stratospheric gravity wave variance, *J. Geophys. Res., 103,* 8627–8640, 1998.

Bailey, P.L., et al., Comparison of cryogenic limb array etalon spectrometer (CLAES) ozone observations with correlative measurements, *J. Geophys. Res., 101,* 9737–9756, 1996.

Barath, F.T., et al., The Upper Atmosphere Research Satellite Microwave Limb Sounder instrument, *J. Geophys. Res., 98,* 10,751–10,762, 1993.

Canziani, P. O. and J. R. Holton, Kelvin waves and the quasi-biennial oscillation: An observational analysis, *J. Geophys. Res., 103,* 31,509–31,521, 1998.

Canziani, P. O., J. R. Holton, E. F. Fishbein, L. Froidevaux and J. W. Waters, Equatorial Kelvin Waves: A UARS MLS View, *J. Atmos. Sci., 51,* 3053–3076, 1994.

Canziani, P. O., J. R. Holton, E. F. Fishbein and L. Froidevaux, Equatorial Kelvin wave variability during 1992 and 1993, *J. Geophys. Res., 100,* 5193–5202, 1995.

CLAES web site, www.lmsal.com/9120/CLAES/dataqual/A.sfdu_for_V9_web_page.htm, accessed 5/30/02.

Considine, D.B., J.E. Rosenfield, and E.L. Fleming, Influence of the Mount Pinatubo aerosol on stratospheric methane and water trends, *J. Geophys. Res., 107,* in press, 200X.

Froidevaux, L., et al., Validation of UARS Microwave Limb Sounder ozone measurements, *J. Geophys. Res., 101,* 10,017–10,060, 1996.

Fujiwara, M., K. Kita, and T. Ogawa, Stratosphere-troposphere exchange of ozone associated with the equatorial Kelvin wave as observed with ozonesondes and radiosondes, *J. Geophys. Res., 103*, 19,173–19,182, 1998.

Fujiwara, M., F. Hasebe, M. Shiotani, N. Nishi, H. Vömel, and S.J. Oltmans, Water vapor control at the tropopause by the equatorial Kelvin wave observed over Galápagos. Submitted to *J. Geophys. Res.,* 2001.

Gille, J.C., et al., Accuracy and precision of the Cryogenic Limb Array Spectrometer (CLAES) temperature retrievals, *J. Geophys. Res., 101,* 9583–9601, 1996.

Holton, J.R., M.J. Alexander, and M.T. Boehm, Evidence for short vertical wavelength Kelvin waves in the Department of Energy-Atmospheric Radiation Measurement Nauru99 radiosonde data, *J. Geophys. Res., 106,* 20,125–20,129, 2001.

Kawamoto, N., M. Shiotani, and J.C. Gille, Equatorial Kelvin waves and corresponding tracer oscillations in the lower stratosphere as seen in LIMS data, *J. Meteorol. Soc. Japan, 75,* 763–773, 1997.

Livesey, N.J., W.G. Read, L. Froidevaux, J.W. Waters, H.C. Pumphrey, D.L. Wu, M.L. Santee, Z. Shippony, R.F. Jarnot, The UARS Microwave Limb Sounder version 5 dataset: Theory, characterization and validation, *J. Geophys. Res.,* in press, 200X.

Mote, P.W., T.J. Dunkerton, and D. Wu, Kelvin waves in stratospheric temperature observed by the Microwave Limb Sounder, *J. Geophys. Res., 107*(D14), 10.1029/2001JD001056, 2002.

Mote, P.W., T.J. Dunkerton, and H.C. Pumphrey, *J. Geophys. Res.,* , this issue, 200X.

Nightingale, R.W., and 12 co-authors, Global CF_2Cl_2 measurements by UARS cryogenic limb array etalon spectrometer: Validation by correlative data and a model, *J. Geophys. Res., 101,* 9711-9736, 1996.

Randel, W.J., Kelvin wave-induced trace constituent oscillations in the equatorial stratosphere. *J. Geophys. Res., 95*, 18,641–18,652, 1990.

Reber, C.A., C.E. Trevathan, R.J. McNeal, and M.R. Luther, The Upper Atmosphere Research Satellite (UARS) Mission, *J. Geophys. Res., 98*, 10,643–10,647, 1993.

Reed, R.J., and C.L. Vlcek, The annual temperature variation in the lower tropical stratosphere, *J. Atmos. Sci. 26,* 163–167, 1969.

Roche, A.E., J.B. Kumer, J.L. Mergenthaler, G.A. Ely, W.G. Uplinger, J.F. Potter, T.C. James, and L.W. Sterritt, The Cryogenic Limb Array Etalon Spectrometer (CLAES) on UARS: Experiment description and performance, *J. Geophys. Res., 98,* 10,763–10,775, 1993.

Roche, A.E., J.B. Kumer, R.W. Nightingale, J.L. Mergenthaler, G.A. Ely, P.L. Bailey, S.T. Massie, J.C. Gille, D.P. Edwards, M.R. Gunson, M.C. Abrams, G.C. Toon, C.R. Webster, W.A. Traub, K.W. Jucks, D.G. Johnson, D.G. Murcray, F.H. Murcray, A. Goldman, and E.C. Zipf, Validation of CH_4 and N_2O measurements by the CLAES instrument on the Upper Atmosphere Research Satellite, *J. Geophys. Res., 101,* 9679–9710, 1996.

Shiotani, M., J.C. Gille, and A.E. Roche, Kelvin waves in the equatorial lower stratosphere as revealed by cryogenic limb array etalon spectrometer temperature data, *J. Geophys. Res., 102*, 26,131–26,140, 1997.

Smith, A.K., P. Preusse, and J. Oberheide, Middle atmosphere Kelvin waves observed in Cryogenic Infrared Spectrometers and Telescopes for the Atmosphere (CRISTA) 1 and 2 temperature and trace species, *J. Geophys. Res., 107*, 10.1029/2001JD000577, 2002.

von Storch, H., and F.W. Zwiers, *Statistical analysis in climate research,* Cambridge University Press, Cambridge, UK, 2001.

Wallace, J.M., and V.E. Kousky, Observational evidence of Kelvin waves in the tropical stratosphere. *J. Atmos. Sci., 25,* 900–907, 1968.

Figure 1. Mean profiles (left column) and standard deviations (right column) of temperature and trace constituents, as indicated, in the tropics (10°S – 10°N).

Figure 2. Time-height plots of the wavenumber-one component (cosine) along the equator of the field indicated. Contour interval for temperature (a,b) is 0.4K; for ozone (c,d), 0.1 ppmv; for methane (e), 0.05 ppmv; for nitrous oxide (f), 8 ppbv; for CFC-12 (g), 25 pptv. Vertical dashed lines denote days when the UARS performed a yaw maneuver; the CLAES instrument was shut off for several days around each yaw day. The mean during each yaw cycle was removed in order to account for a small yaw-dependent bias, which mainly affected CLAES ozone.

Figure 3. Spectral power (K^2) of variations in temperature from the MLS instrument, viewed as functions of (a) period, (b) zonal wavenumber, (c) latitude, and (d) altitude. In panel (a), power along the equator has been summed over altitude and over positive zonal wavenumbers, then smoothed once with a 1-2-1 filter. Power drops to zero near the limits of the bandpass filtering (4–90 days). In panel (b), power along the equator in the 5-30 day frequency band has been summed in altitude. In panel (c), power for zonal wavenumber 1 ($k = 1$) has been summed in altitude and over the 5-30 day frequency band. Panel (d) shows spectral power at the equator for $k = 1$ summed over the 5-30 day frequency band (solid) and over the 4–90 day band (dashed).

Figure 4. As in Figure 3 but for MLS ozone ($ppmv^2$).

Figure 5. Squared coherence of temperature and ozone as a function of altitude and period (a), and the phase for the spectral bands 8–11 days (b) and 5–7 days (c).

Figure 6. The field indicated in each panel's title has been regressed on a reference time series, the first principal component of extended EOF of MLS temperature (see text for details). Approximate phase lines are indicated in each panel; they have been derived from panel *a* by calculating best-fit lines to the profile maximum and minimum at each longitude. Panel *a* shows MLS temperature data, and reproduces Figure 7a of M02; *b*: as in *a* but for CLAES temperature data. Contour interval in panels *a* and *b* is 0.15K. Panels *c* and *d* show ozone data from MLS and CLAES, respectively; contour interval 0.025 ppmv. Panels $e - g$ show CLAES methane (contour interval 4 ppbv), nitrous oxide (1 ppbv), and CFC-12 (1 pptv). Values plotted are derived from dimensionless reference time series, but a fluctuation of 1K in panel *a* corresponds roughly to 0.15 ppmv in ozone, 30 ppbv in methane, 7 ppbv in nitrous oxide, and 7 pptv in CFC-12.

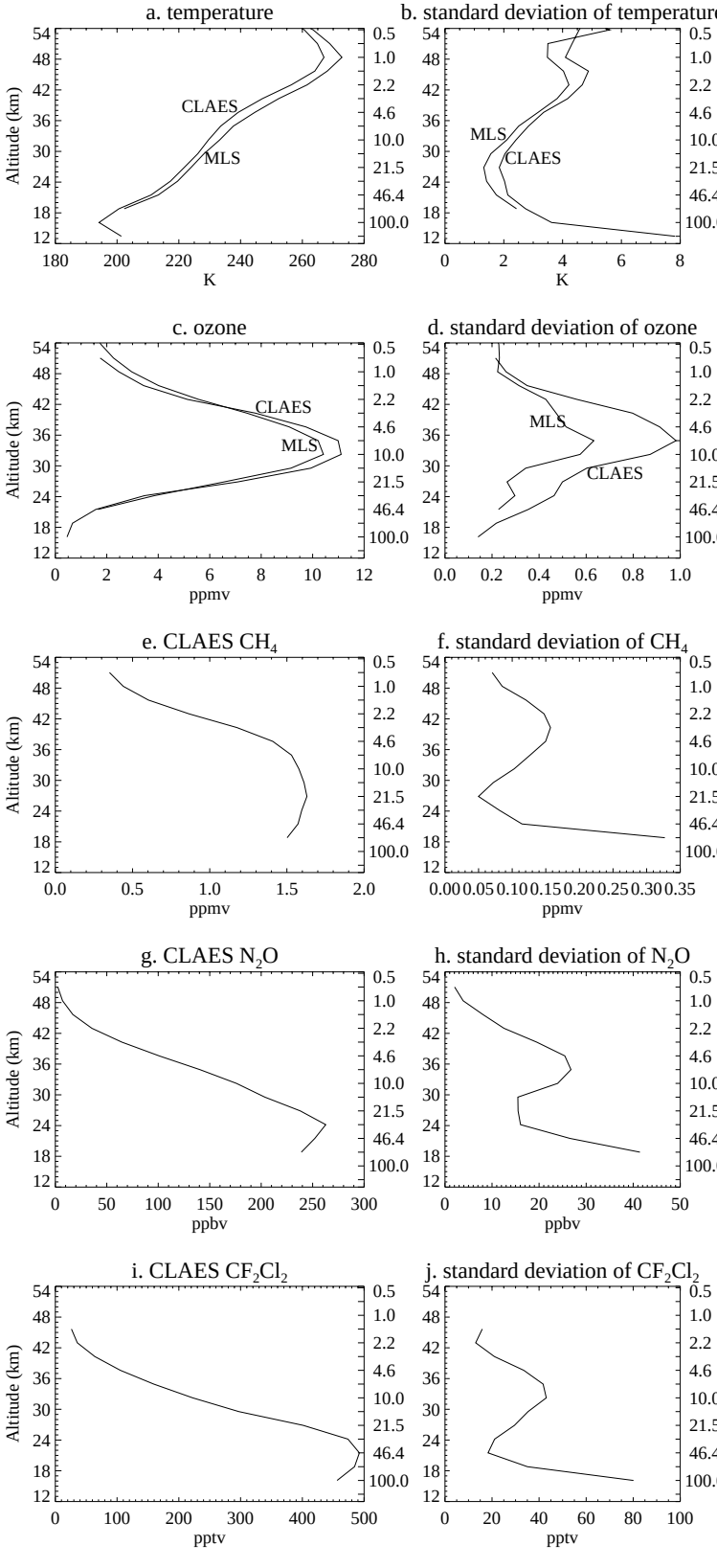
a. temperature
b. standard deviation of temperature
c. ozone
d. standard deviation of ozone
e. CLAES CH_4
f. standard deviation of CH_4
g. CLAES N_2O
h. standard deviation of N_2O
i. CLAES CF_2Cl_2
j. standard deviation of CF_2Cl_2
Altitude (km)
CLAES
MLS
K
ppmv
ppbv
pptv

a. MLS temperature

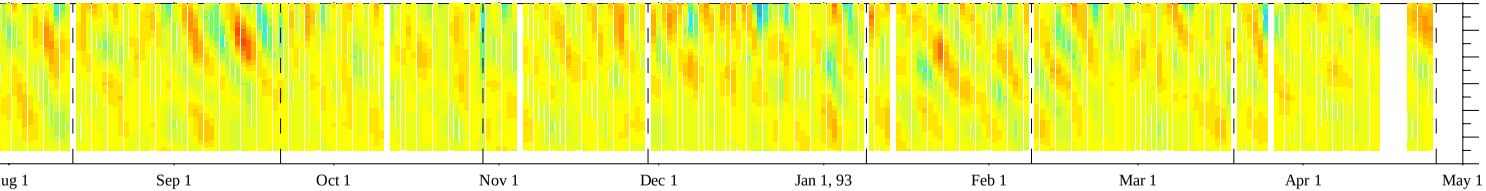

b. CLAES temperature

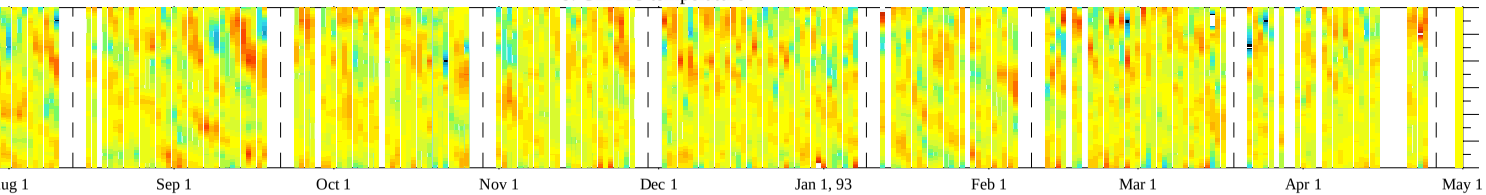

c. MLS ozone

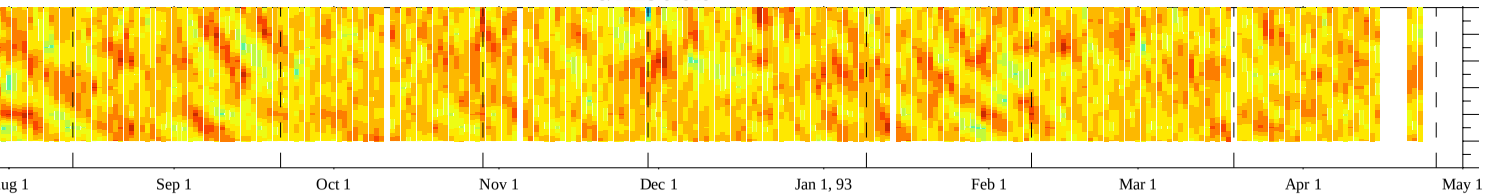

d. CLAES ozone

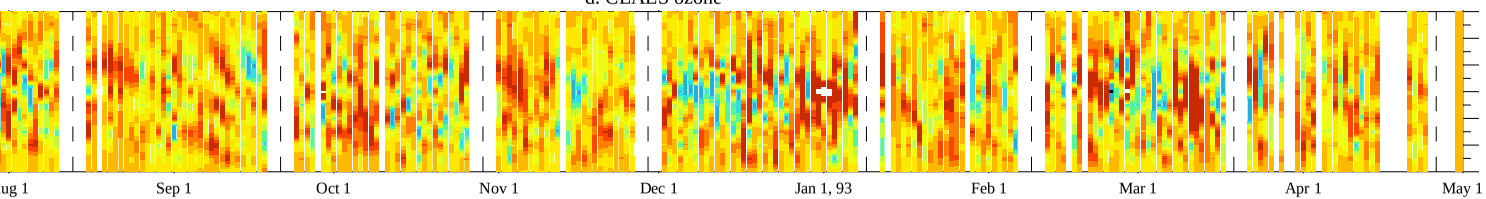

e. CLAES methane

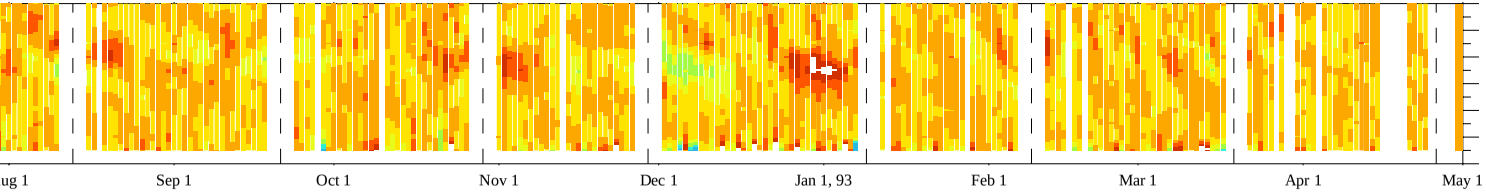

f. CLAES nitrous oxide

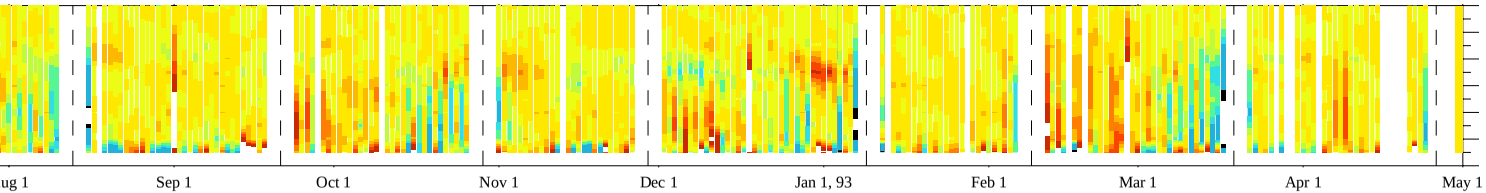

g. CLAES CFC-12

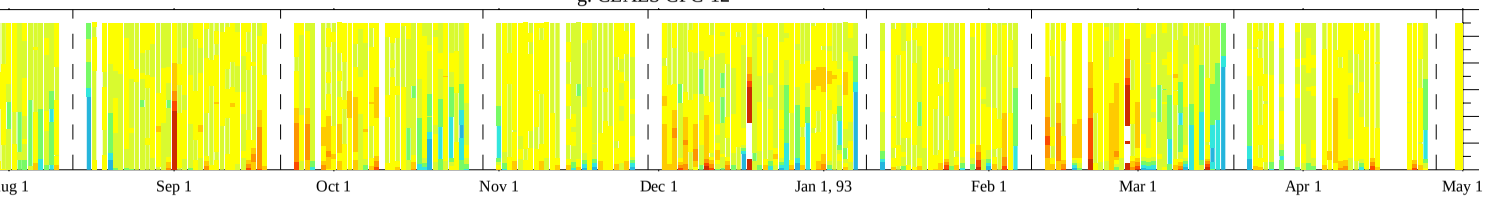

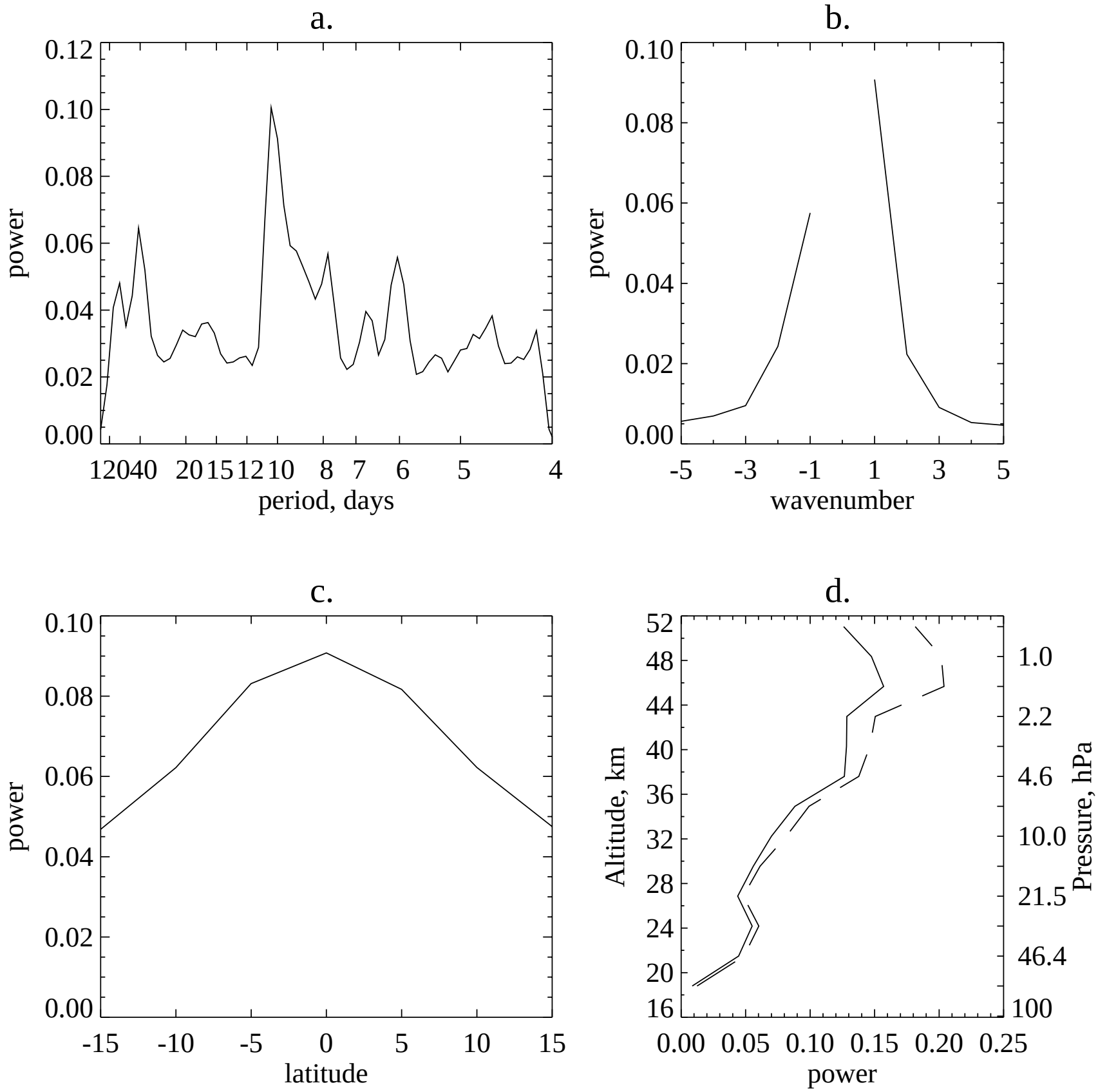
a.
power
0.12
0.10
0.08
0.06
0.04
0.02
0.00
120 40 20 15 12 10 8 7 6 5 4
period, days
b.
power
0.10
0.08
0.06
0.04
0.02
0.00
-5 -3 -1 1 3 5
wavenumber
c.
power
0.10
0.08
0.06
0.04
0.02
0.00
-15 -10 -5 0 5 10 15
latitude
d.
Altitude, km
52
48
44
40
36
32
28
24
20
16
Pressure, hPa
1.0
2.2
4.6
10.0
21.5
46.4
100
0.00 0.05 0.10 0.15 0.20 0.25
power

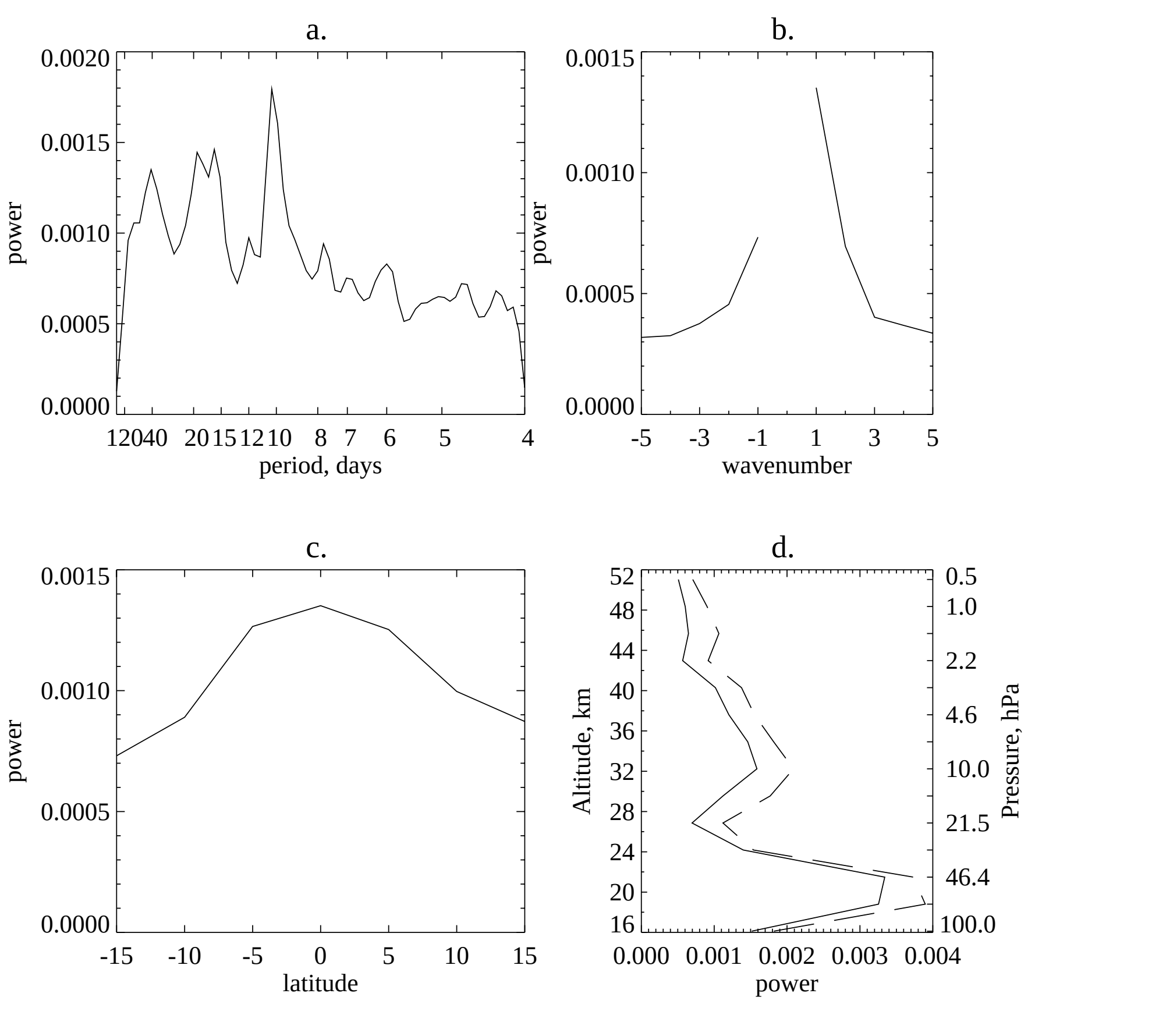
a.
0.0020
0.0015
0.0010
0.0005
0.0000
power
120
40
20
15
12
10
8
7
6
5
4
period, days
b.
0.0015
0.0010
0.0005
0.0000
power
-5
-3
-1
1
3
5
wavenumber
c.
0.0015
0.0010
0.0005
0.0000
power
-15
-10
-5
0
5
10
15
latitude
d.
52
48
44
40
36
32
28
24
20
16
Altitude, km
0.5
1.0
2.2
4.6
10.0
21.5
46.4
100.0
Pressure, hPa
0.000
0.001
0.002
0.003
0.004
power

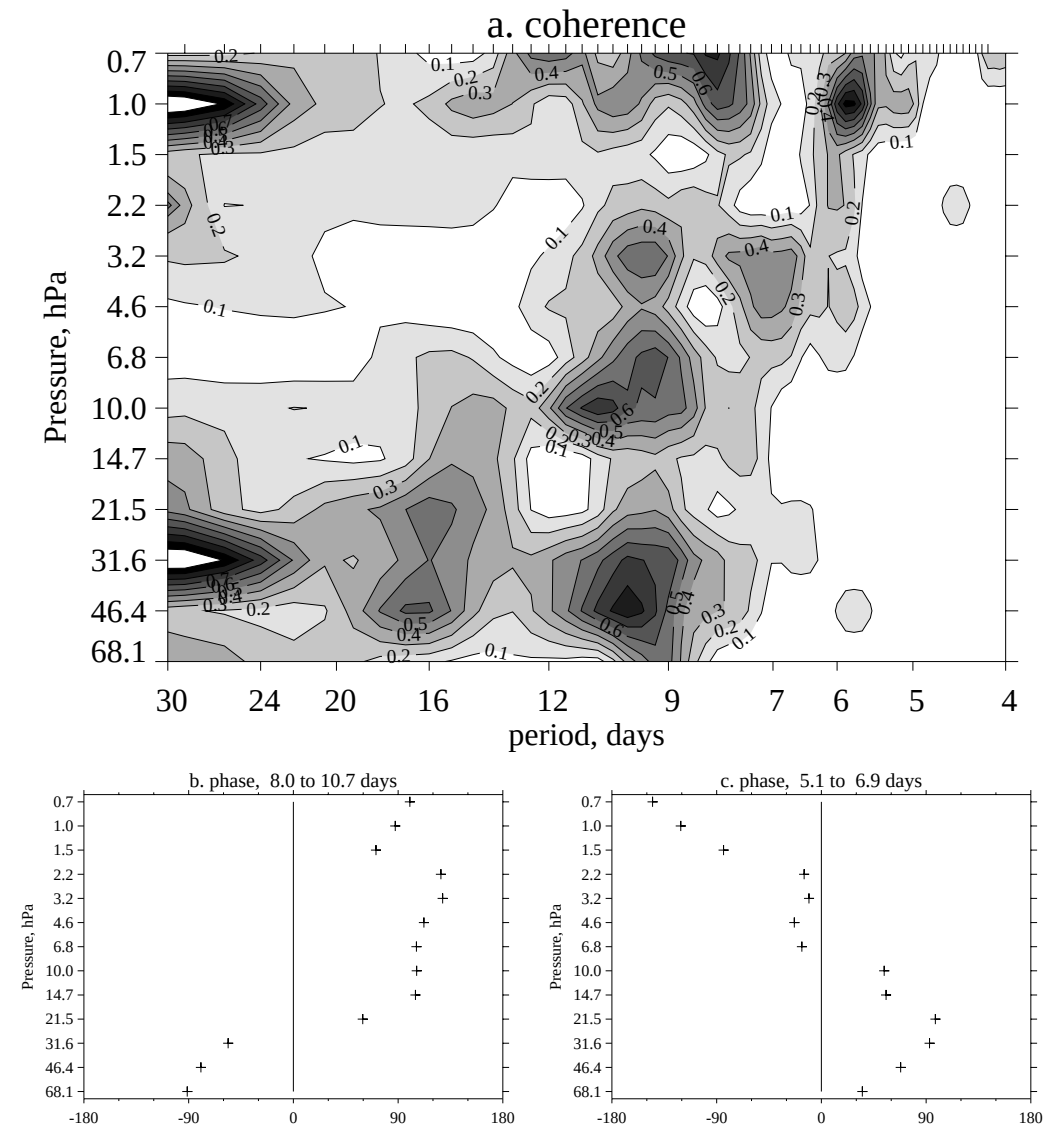
a. coherence
Pressure, hPa
0.7
1.0
1.5
2.2
3.2
4.6
6.8
10.0
14.7
21.5
31.6
46.4
68.1
30
24
20
16
12
9
7
6
5
4
period, days

b. phase, 8.0 to 10.7 days
Pressure, hPa
0.7
1.0
1.5
2.2
3.2
4.6
6.8
10.0
14.7
21.5
31.6
46.4
68.1
-180
-90
0
90
180

c. phase, 5.1 to 6.9 days
Pressure, hPa
0.7
1.0
1.5
2.2
3.2
4.6
6.8
10.0
14.7
21.5
31.6
46.4
68.1
-180
-90
0
90
180

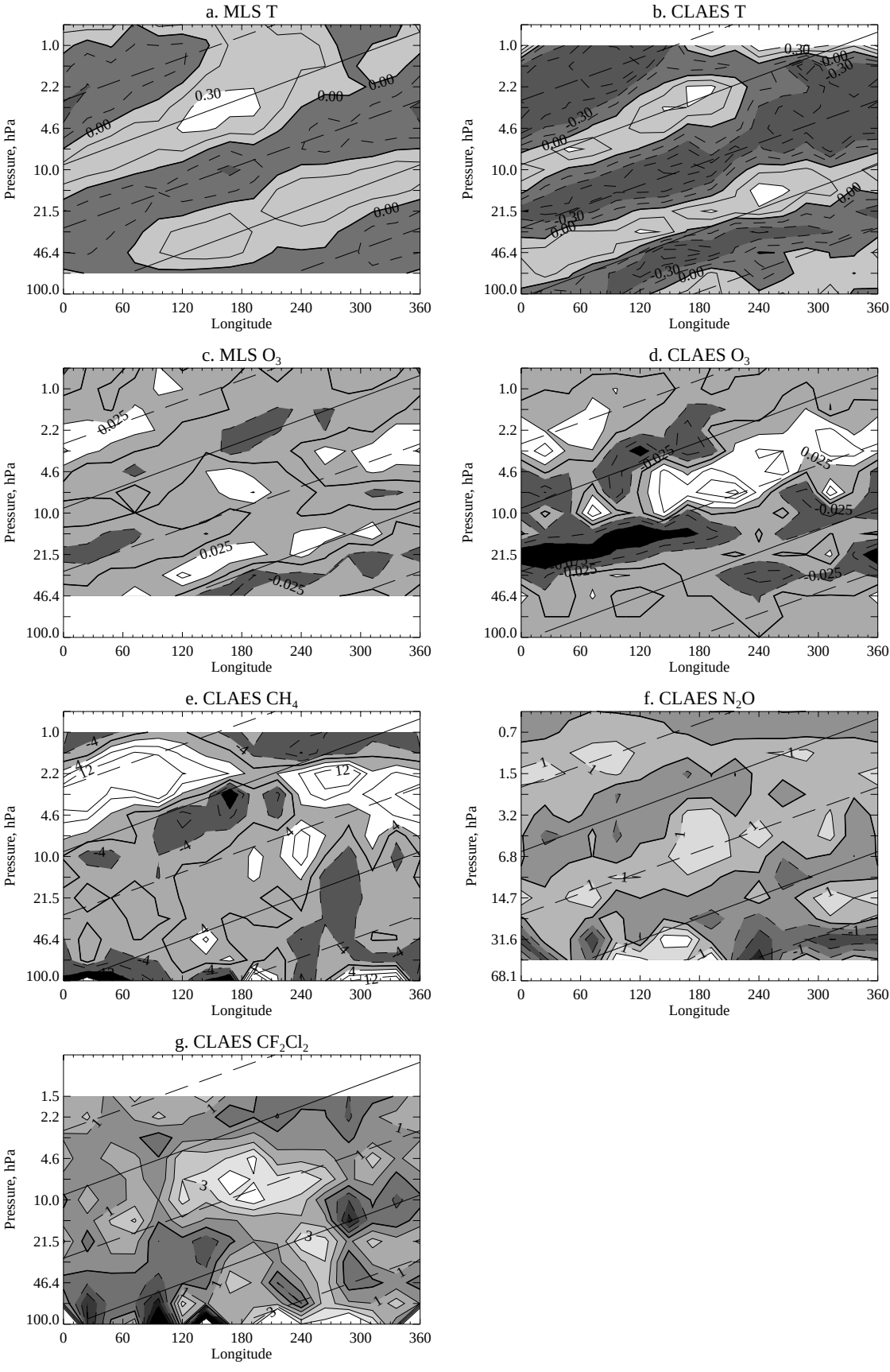
a. MLS T
b. CLAES T
c. MLS O_3
d. CLAES O_3
e. CLAES CH_4
f. CLAES N_2O
g. CLAES CF_2Cl_2
Pressure, hPa
Longitude
1.0
2.2
4.6
10.0
21.5
46.4
100.0
0.7
1.5
3.2
6.8
14.7
31.6
68.1
0
60
120
180
240
300
360